RESEARCH ARTICLE

NANO · MICRO small
www.small-journal.com

Needlestick-Stimulation-Induced Conversion of Short-Wave Infrared-Light Transparency Using a Liquescent Radical Anion

*Ruifeng Shu, Takeshi Naota, and Shuichi Suzuki**

A liquescent salt consisting of a 7,7,8,8-tetracyanquinodimethane (TCNQ) radical anion and a tetra-*n*-decylammonium ion, 1^+●$TCNQ^{\bullet-}$, exhibits rapid changes in the short-wave infrared (SWIR) light transparency at 1000–1400 nm upon the application of a one-shot needlestick-stimulus. Radical anion salt 1^+●$TCNQ^{\bullet-}$ transforms from a blue solid to a green liquid at 90 °C without decomposition under aerated conditions, and remains in the liquid state upon cooling to 70 °C. After applying pressure with a needlestick on a cover glass at 70 °C, the liquid transforms rapidly into the solid state over a timescale of seconds across a centimeter scale of area. Along with the liquid–solid transition, the SWIR-light transparency at 1200 nm completely switches from the "on" to the "off" states. Experimental results, such as electronic spectra and crystal structure analysis, indicates that the SWIR-light absorption in the solid state is due to the existence of a slipped-stacking π-dimer structure for $TCNQ^{\bullet-}$. The rapid rearrangement is induced by the formation of the π-dimer structures from the monomers of $TCNQ^{\bullet-}$ and the subsequent generations of the solid-state seed.

1. Introduction

Open-shell organic molecules and their assemblies have drawn considerable interests as promising components for intriguing functional materials because of their spin characteristics, redox properties, and narrow band gaps.[1–6] They are widely used in molecule-based magnets,[1] electrical conductors,[2] radical-based batteries,[3] organic-based high-spin compounds,[4] magnetoluminescent materials,[5] and dyes/pigments that absorb in near-infrared (NIR: 700–1000 nm) and short-wave infrared (SWIR: 1000–2500 nm) light regions.[6] Recent research has been directed towards the molecule-based system, wherein the NIR/SWIR transparency can be modulated even in the condensed states.[7–10] This is achieved by changing temperature,[8] applying mechanostress,[9,10] and exposing solvent vapor,[10] using open-shell molecular systems in which photophysical properties vary remarkably depending on the associated structures, such as monomer, σ-bonded and π-bonded dimer (π-dimer). However, these stimuli-responsive materials generally required the application of prolonged stimulations to change the entire areas of the materials (**Figure 1a**), owing to the restricted conformational and translational motions of the molecular units in the condensed states. Additionally, the stimulated materials required dissolution using appropriate solvent to return them to their initial states (Figure S1a, Supporting Information). Here, we have attempted to establish a method to overcome the restrictions in the molecular motions, even in the condensed state, and promote changes in their alignments in the entire system triggered by a one-shot and indirect stimulation (Figure 1b; Figure S1b, Supporting Information), as reported for stimuli-responsible luminescent materials.[11] These systems have potential application in a completely new type of dyes/pigments controllable physical properties related on the NIR/SWIR light for realizing further sophisticated optical filters,[7,12] high-security inks,[13] and multichannel materials associated with their spin properties.[14]

To realize such unprecedented sensitive materials, it is necessary to design duality states in which the starting state is flexible enough to allow the changes in the alignments of molecules in the condensed state, but the stimulated positions can change to ordered aggregates and then rapidly spread to the whole area. In this study, a 7,7,8,8-tetracyanoquinodimethane (TCNQ) radical anion,[15] which can assemble into a dimer structure, was utilized to attempt the modulation of the SWIR-light transparency. Consequently, we found that a liquescent salt consisting of a TCNQ radical anion and a tetra-*n*-decylammonium ion, $\mathbf{1^+}$●$\mathbf{TCNQ^{\bullet-}}$ (**Figure 2a**), displayed drastic and rapid conversion of the SWIR-light transparency during the liquid–solid phase transition upon the application of a one-shot stimulation with a needlestick (Figure 2b). We consider that these molecular architectures showcase

R. Shu, T. Naota, S. Suzuki
Department of Chemistry, Graduate School of Engineering Science
Osaka University
Toyonaka, Osaka 560-8531, Japan
E-mail: suzuki-s@chem.es.osaka-u.ac.jp

The ORCID identification number(s) for the author(s) of this article can be found under https://doi.org/10.1002/smll.202311557

DOI: 10.1002/smll.202311557

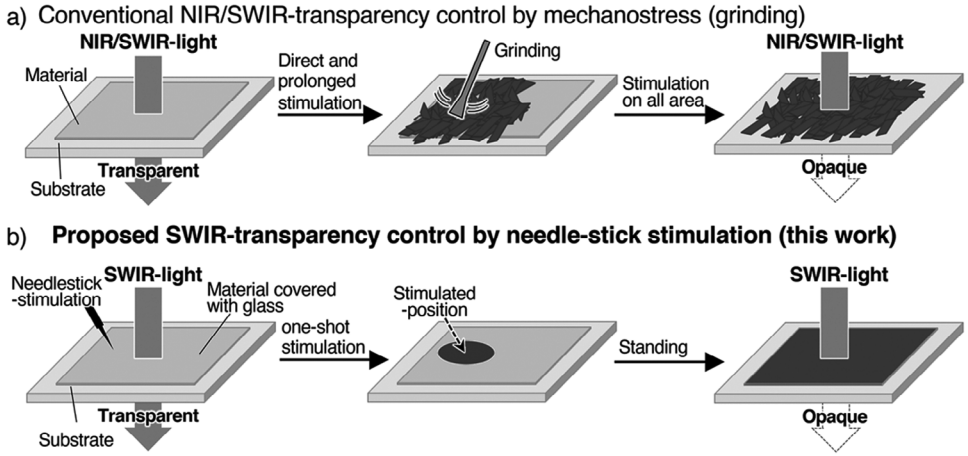

Figure 1. Schematic representations for controlling photophysical properties in the NIR/SWIR region (NIR: 700–1000 nm; SWIR: 1000–2500 nm) using a) the conventional and b) the proposed materials, respectively.

promising potential for the innovative advancement of wearable technologies.[16]

2. Results and Discussion

Differential scanning calorimetry measurements and visual observations revealed that $\mathbf{1}^{+}\bullet\mathbf{TCNQ}^{\bullet-}$ underwent intriguing phase transitions during heating and cooling processes (**Figure** 3a; Figure S2, Supporting Information). Radical anion salt $\mathbf{1}^{+}\bullet\mathbf{TCNQ}^{\bullet-}$, obtained as a blue solid by recrystallization from dichloromethane and diethyl ether, was transformed into a green liquid upon heating to 89–90 °C (melting point: T_m), remained in the liquid state upon cooling until 59–60 °C (freezing point: T_f), and then returned to the initial blue solid form. Thermogravimetric analysis revealed no weight losses until over 250 °C under aerated conditions (Figure 3b), indicating that $\mathbf{1}^{+}\bullet\mathbf{TCNQ}^{\bullet-}$ did not decomposed even in the liquid state. Previously, it was reported that salts of $\mathbf{TCNQ}^{\bullet-}$ with $(n\mathrm{C_mH_{2m+1}})_4\mathrm{N}^+$ (m = 2–12) were melted at below 250 °C[17] and $(n\mathrm{C_4H_9})_4\mathrm{N}^+\bullet\mathbf{TCNQ}^{\bullet-}$ was decomposed at 135 °C.[15a] Additionally, it was also reported that salts of $\mathbf{TCNQ}^{\bullet-}$ and 1-ethyl-3-methylimidazolium or 1-butyl-3-methylimidazolium ion exhibited low melting points (145 and 155 °C) without decomposition under inert atmosphere.[18] These results indicated that the melting point of $\mathbf{1}^{+}\bullet\mathbf{TCNQ}^{\bullet-}$ was quite lower than those of reported $\mathbf{TCNQ}^{\bullet-}$ salts.

Electronic spectra of $\mathbf{1}^{+}\bullet\mathbf{TCNQ}^{\bullet-}$ in the blue solid and green liquid states indicated that the photophysical properties were completely different in the visible, NIR, and SWIR regions. In the blue solid state, $\mathbf{1}^{+}\bullet\mathbf{TCNQ}^{\bullet-}$ exhibited robust absorption in the SWIR region at λ_{max} = 1085 nm, with absorption bands at λ_{max} = 653 and 391 nm (**Figure** 4a(I)). In the green liquid state, generated by heating over T_m, the strong SWIR-light absorption of the material disappeared drastically in the electronic spectrum, but there was intense absorption between the NIR and visible regions, at λ_{max} = 855, 759, and 409 nm (Figure 4a(II)). The electronic spectrum of the material in the liquid state was similar to that of $\mathbf{1}^{+}\bullet\mathbf{TCNQ}^{\bullet-}$ in the dilute solution state (Figure S3, Supporting Information), strongly suggesting that the $\mathbf{TCNQ}^{\bullet-}$ species formed a monomer structure in the green liquid state. The electronic spectrum of the solid generated by cooling to T_f was similar to that of the initial blue solid state (Figure S4,

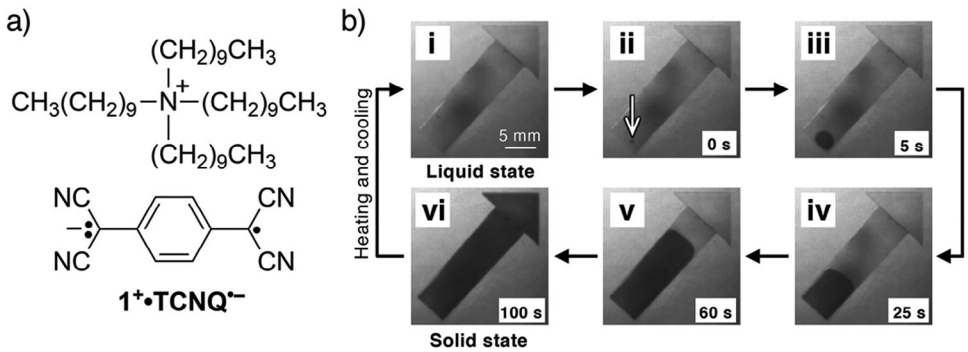

Figure 2. a) Chemical structure of $\mathbf{1}^{+}\bullet\mathbf{TCNQ}^{\bullet-}$. b) Time-dependent SWIR images of the $\mathbf{1}^{+}\bullet\mathbf{TCNQ}^{\bullet-}$ thin film using an SWIR-detection camera under 1200 nm light irradiation at 70 °C; the white and black colors denoted the transparent and opaque states under 1200 nm light, respectively. (i) Liquid $\mathbf{1}^{+}\bullet\mathbf{TCNQ}^{\bullet-}$ was placed on the glass plate and covered with a glass. (ii) One-shot and weak stimulation was applied at the white arrow position over the cover glass. (iii, vi) The material was left without any stimulations at 70 °C. The solid state (vi) was converted to the liquid state (i) by heating to 90 °C and cooling to 70 °C.

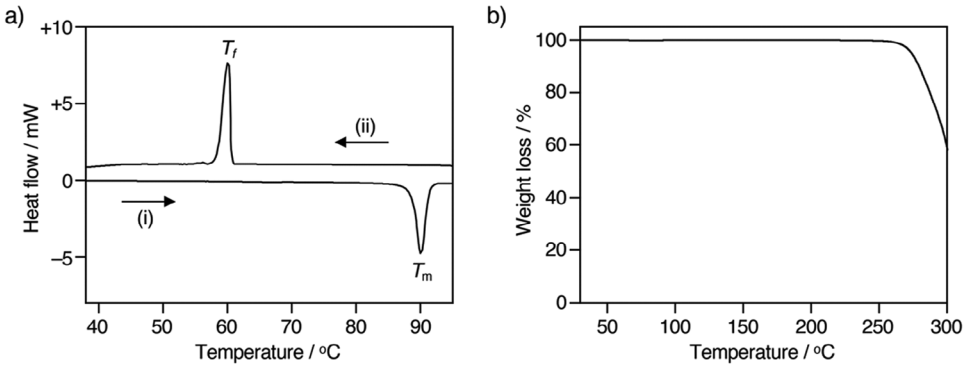

Figure 3. a) Differential scanning calorimetry diagram of **1**$^{+}$●**TCNQ**$^{\bullet-}$ on (i) heating and (ii) cooling processes (scan rate: 5 °C min^{-1}). T_m and T_f denote the melting and freezing points, respectively. b) Thermogravimetric analysis diagram of **1**$^{+}$●**TCNQ**$^{\bullet-}$ (scan rate: 20 °C min^{-1}).

Supporting Information), and these changes were consistently observed during phase transitions. Notably, the SWIR band was not observed in the solution state, indicating that the band at λ_{max} = 1085 nm in the blue solid state is derived from the associated structure of the **TCNQ**$^{\bullet-}$ species. The electron spin resonance (ESR) spectra of **1**$^{+}$●**TCNQ**$^{\bullet-}$ provided more information about the associated structures in the solid and liquid states. The ESR signal corresponding to the **TCNQ**$^{\bullet-}$ species appeared upon the phase transition from the blue solid to the green liquid state (Figure 4b). The significant lower intensity of the ESR signals at 30 °C than that in the liquid state at 100 °C indicated that **TCNQ**$^{\bullet-}$ formed a singlet dimer structure in the solid state. A careful investigation of the ESR spectra in the solid state further revealed that signals originating from thermally excited triplet species of **TCNQ**$^{\bullet-}$ dimer were observed at 30 °C in the spin-allowed and spin-forbidden regions (Figure S5, Supporting Information). The singlet–triplet gap was estimated to be ≈−1.7 × 10^3 K using the singlet–triplet model from the temperature dependence of the signal intensities (Figure S6, Supporting Information), indicating that the **TCNQ**$^{\bullet-}$ units formed a dimer structure with the strong antiferromagnetic spin–spin interactions.

Single-crystal X-ray diffraction was performed to determine the dimer structure of the radical anion units of **1**$^{+}$●**TCNQ**$^{\bullet-}$ (**Figure 5**). The analysis revealed that the **TCNQ**$^{\bullet-}$ species formed a π-dimer with a slipped-stacking arrangement. The intermolecular distance of the intra-π-dimer was estimated to be 3.20 Å, which is shorter than the sum of the van der Waals radii for the carbon atoms (3.40 Å).[19] Packing revealed no significant inter-dimer contacts in any of the axis projections (Figure S7, Supporting Information). Therefore, the strong absorption of **1**$^{+}$●**TCNQ**$^{\bullet-}$ in the blue solid state in the SWIR region with considerably low ESR intensities is attributed to the formation of the slipped-stacking π-dimer structure. Density functional theory calculations of the slipped-stacking π-dimer structure also suggest the similar photophysical and magnetic properties (Figure S8, Table S1, Supporting Information).

Interestingly, we found that the green liquid state of **1**$^{+}$●**TCNQ**$^{\bullet-}$ immediately transformed into its blue solid state, accompanied by drastic changes in the SWIR-light

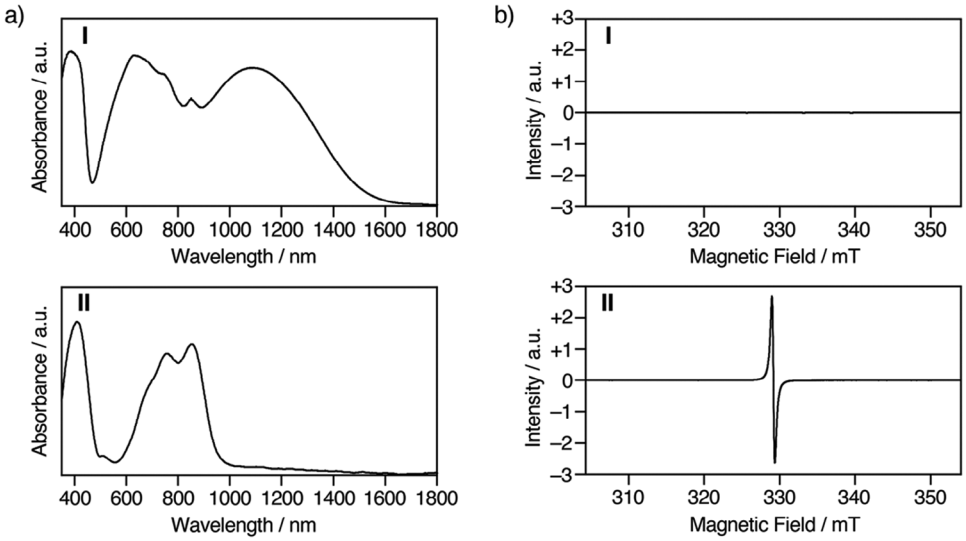

Figure 4. a) Electronic spectra of **1**$^{+}$●**TCNQ**$^{\bullet-}$ in (I) the solid state at 25 °C (KBr pellet) and (II) the liquid state at 100 °C (thin film placed on quartz glasses). b) ESR spectra of **1**$^{+}$●**TCNQ**$^{\bullet-}$ in (I) the solid state at 30 °C and (II) the liquid state at 100 °C.

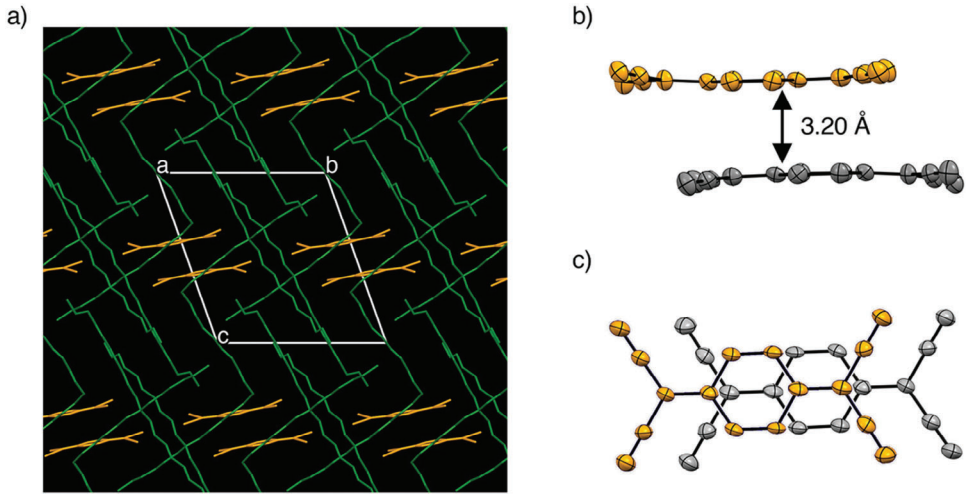

Figure 5. a) Packing of $\mathbf{1}^{+}\bullet\mathbf{TCNQ}^{\bullet-}$ along the *a*-axis. Units of $\mathbf{TCNQ}^{\bullet-}$ and $\mathbf{1}^{+}$ are represented by orange and green, respectively. b) Side and c) top ORTEP views for the π-dimer structure of $\mathbf{TCNQ}^{\bullet-}$. Thermal ellipsoids are drawn at the 50% probability level. The units at the upper and forefront positions in the dimer are represented by the orange color.

absorption, when an indirect one-shot stimulus was applied without cooling to T_f, as visualized using an SWIR imaging camera under 1200 nm light (Figure 2b; Movie S1, Supporting Information). Liquid $\mathbf{1}^{+}\bullet\mathbf{TCNQ}^{\bullet-}$ at 70 °C, prepared by cooling the melted state generated above T_m, was adjusted to the shape of an arrow using a cover glass. Before stimulation, the material was transparent to the SWIR light at 1200 nm (Figure 2b (i)). After applying a one-shot weak stimulation with the tip of a steel needle on the cover glass, an SWIR-light–opaque domain was generated at the location of the trigger (Figure 2b (ii)). Subsequently, a process to the opaque state propagated away from the stimulation point (Figure 2b (iii, vi)). The change along the 25-mm arrow-shape cover glass took 100 s to complete, demonstrating that the propagation rate was ≈15 mm min^{-1}. We reported changes in the magnetic and NIR absorption properties of the solid of *N*-penthylphenothazine radical cation with bis(*N*-trifluoromethanesulfonyl)imide ion by needlestick stimulation at 50 °C. The rate was estimated to be ≈0.4 mm min^{-1}, which was slower than the present system.[9d]

We found that needlestick stimulation at any position could initiate the changes in the SWIR-light transparency. The liquid state of $\mathbf{1}^{+}\bullet\mathbf{TCNQ}^{\bullet-}$ at 70 °C covered by a round glass was subjected to three-time stimulations (**Figure 6**a, Movie S2, and Figure S9, Supporting Information). It was observed that the change from transparent to opaque states under the SWIR light started from the stimulated positions, independent of time and the positions. Notably, the weak SWIR-light absorption state remained unchanged without stimulation for several hours at 70 °C (Figure 6a; Figure S9, Supporting Information). The transparent state under the SWIR light could be regenerated by heating the material to T_m. Thus, using the system, the SWIR-light transparency could be modulated repeatedly.

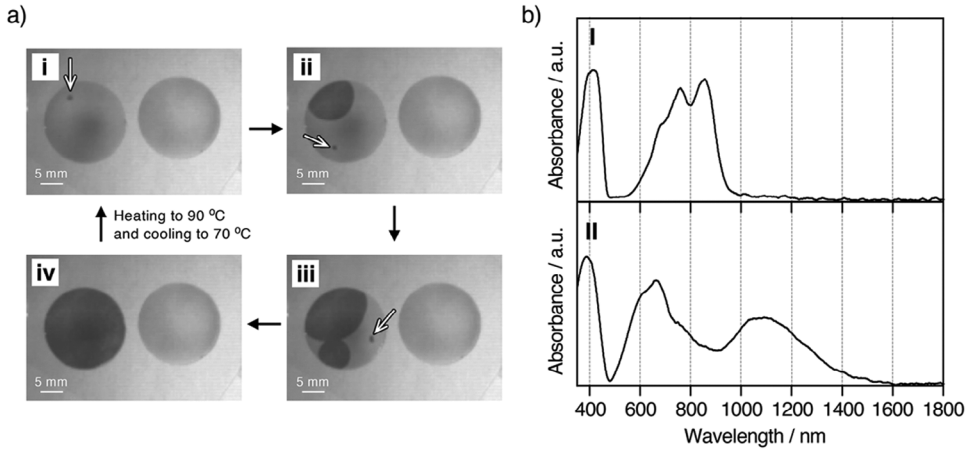

Figure 6. a) SWIR images of the $\mathbf{1}^{+}\bullet\mathbf{TCNQ}^{\bullet-}$ thin film under 1200 nm light at 70 °C; the white and black colors denoted the transparent and opaque states under 1200 nm light, respectively. Liquid $\mathbf{1}^{+}\bullet\mathbf{TCNQ}^{\bullet-}$ was placed on the glass plate at two positions and covered with round-shaped glasses. Three one-shot stimulations over the cover glass were applied to sample on the left side at the white arrow position, whereas no stimulations were applied to the sample on the right. b) Electronic spectra at 70 °C (I) before and (II) after stimulation, respectively.

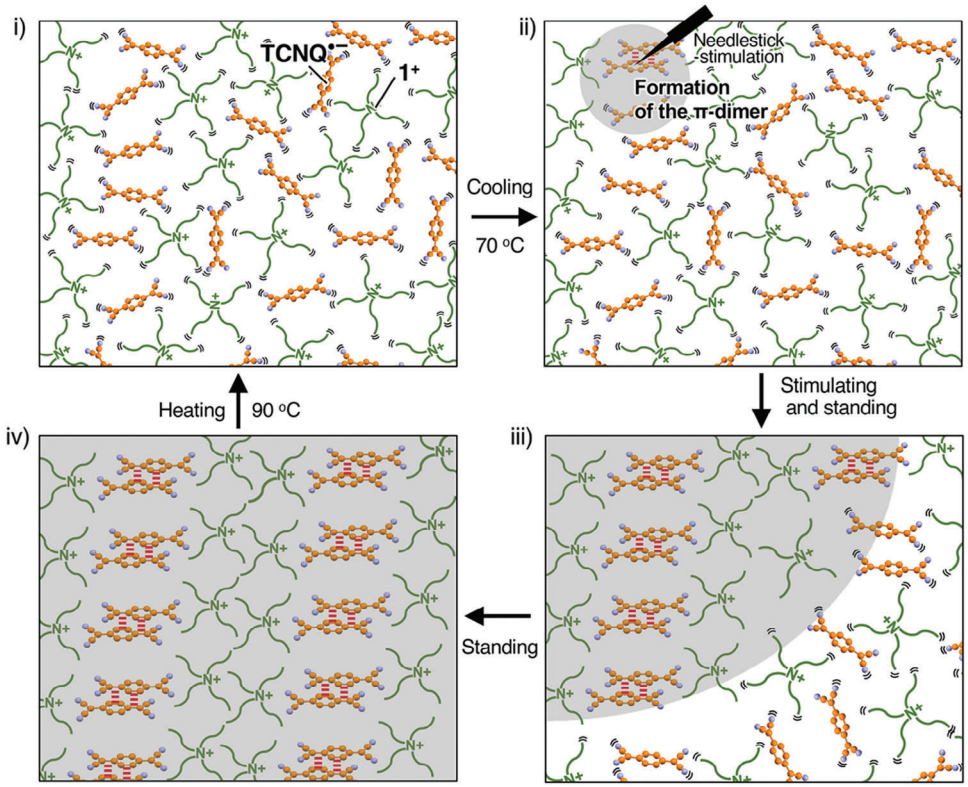

Figure 7. Proposed aggregation structures during the changes in the SWIR-light transparent properties of liquescent for **1**$^{+}$●**TCNQ**$^{\bullet-}$: i) Initial liquid state after melting, ii) formations of π-dimers with the SWIR-light absorption (shown in gray color) after the needlestick stimulation, iii) intermediate state during the growth of the SWIR-light absorption domain, and iv) the final solid state. The broken lines in red represent the intra-π-dimer interactions.

The electronic spectra of **1**$^{+}$●**TCNQ**$^{\bullet-}$ before and after stimulation provided crucial information for the changes in the associated structures of **TCNQ**$^{\bullet-}$ (Figure 6b). The electronic spectrum at 70 °C before stimulation (Figure 6b (I)) was similar to that of the liquid state at 100 °C (Figure 4a (II)), indicating that **TCNQ**$^{\bullet-}$ existed as a monomer species. After stimulation and complete phase change, the electronic spectrum of the material at 70 °C (Figure 6b (II)), exhibiting strong absorption in the NIR/SWIR region at λ_{max} = 1091 nm, was similar to that in the initial blue solid state at 25 °C (Figure 4a (I)). With the slight changes in the visible light region, the color of **1**$^{+}$●**TCNQ**$^{\bullet-}$ changed from green to blue (Figure S10, Supporting Information). The change in the electronic spectra indicated that the needlestick stimulation induced the transformation to the slipped-stacking π-dimer structures, as suggested by the XRD analysis.

The stimulation-induced SWIR-light transparency conversion using **1**$^{+}$●**TCNQ**$^{\bullet-}$ can be explained by the following mechanism (**Figure 7**). The liquid salt exhibited an SWIR-transparent and ESR-active state because the **TCNQ**$^{\bullet-}$ species existed as monomer units. They could remain in the liquid state at temperature lower than T_m, which is attributed to the high conformational flexibility of tetra-*n*-decylammonium ions. Upon needlestick stimulation at the appropriate temperature, the liquid state underwent rearrangement from the monomer to the slipped-stacking π-dimer units, which induced the formation of a solid-state domain with strong SWIR-light absorption. We speculate that the change in liquid flow before and after the needlestick stimulation resulted in the formation of a solid-state domain of the slipped-stacking π-dimer structures. The growth of the solid-state domain caused molecular aggregation, and the liberated ion pairs in the liquid state underwent an ordered rearrangement centered on the solid-state domain. Subsequently, the conformational and translational motions of the decyl groups of the ammonium ions on and near the solid-state domain were inhibited, which accelerated the associations of the liberated ion pairs in the liquid state and extended the solid-state domain. Ultimately, the entire system transformed into the SWIR-opaque solid state with the π-dimer structures. Polarized optical microscopy images at the location of the one-shot stimulation indicated that the molecular association spread in all directions around the trigger position (Figure S11, Supporting Information). The directions of solid growth could be discerned by the texture, which was not observed in the solid formed by temperature-dominated liquid–solid phase transitions (Figure S11, Supporting Information), suggesting that the phase transition induced by needlestick-stimulation was an ordered rearrangement, as described in the assumed mechanism.

3. Conclusion

We have designed a liquescent radical anion salt, **1**$^{+}$●**TCNQ**$^{\bullet-}$, which displayed drastic changes in its photophysical properties in the visible, NIR, and SWIR-light regions upon the application of a weak and one-shot stimulation with a needlestick. An

unprecedented enhancement in the SWIR-light absorption was achieved by controlling the monomer–dimer transition of the radical anions even in the condensed state. Further investigations of liquescent $TCNQ^{\bullet-}$ salts having other counter cations are underway to clarify their intriguing phase transitions. We are currently attempting to verify whether magnetic fields and light irradiation also cause changes in the photophysical, magnetic, and related functional properties of liquescent radical salts.

4. Experimental Section

General: Melting points were measured in glass plates on a Yanagimoto melting point apparatus. IR spectra were recorded on JASCO FT/IR-400 using KBr pellets. The elemental analyses were performed at the Analytical Instrument Facility, Graduate School of Science, Osaka University. SWIR images were captured by an ARTRAY ARTCAM-0016TNIR InGaAs camera equipped with a LM25HC-SW lens under 1200-nm light (generated from halogen light source through a band-pass filter of 1200 nm). Electronic spectra were obtained on a Hitachi U-4100 spectrometer and a JASCO V-770 spectrometer. Variable-temperature electronic spectra were carried out using a glass heater. The thermal gravimetry thermal gravimetric analyses were performed by a Hitachi NEXTA STA. Mass spectra were recorded on a JMS-AX700 spectrometer with NBA matrix. Differential scanning calorimetry was performed with a SHIMADZU DSC-60. Single-crystal X-ray data of $\mathbf{1}^{+}\bullet\mathbf{TCNQ}^{\bullet-}$ were collected by a Rigaku XtaLAB P200 diffractometer with graphite monochromated Mo-Kα radiation (λ = 0.71075 Å) at 113 K (−160 °C). ESR spectra were recorded with a JEOL JES-FE2XG spectrometer. The polycrystalline samples were used for the measurements of ESR spectra. The polycrystals of $\mathbf{1}^{+}\bullet\mathbf{TCNQ}^{\bullet-}$ were placed in an ESR tube. The tube was degassed under reduced pressure and then filled by argon before the measurements of (VT-)ESR spectra. The parameters for the ESR measurements were as follows: Solid state at 30 °C: microwave power 1 mW, modulation width 1 × 0.1 mT, amplitude 1 × 100, time constant 0.03 s; Liquid state at 100 °C: microwave power 1 mW, modulation width 1 × 0.01 mT, amplitude 1 × 1, time constant 0.03 s.

7,7,8,8-Tetracyanoquinodimethane (TCNQ), tetra-*n*-decylammonium bromide, methanol (MeOH), dehydrated dichloromethane (CH_2Cl_2), and diethyl ether (Et_2O) were commercially available and used without further purification. Lithium–7,7,8,8-tetracyanoquinodimethane radical anion ($\mathbf{Li}^{+}\bullet\mathbf{TCNQ}^{\bullet-}$) was prepared according to the literature.[15a]

Synthesis of $\mathbf{1}^{+}\bullet\mathbf{TCNQ}^{\bullet-}$: An aqueous solution (10 mL) of $\mathbf{Li}^{+}\bullet\mathbf{TCNQ}^{\bullet-}$ (43 mg, 0.20 mmol) was slowly added to a MeOH solution (20 mL) of tetra-*n*-decylammonium bromide (132 mg, 0.20 mmol). The mixture was stirred for 15 min at room temperature. Then, the precipitate was collected by filtration, washed with water, and dried in *vacuo*. The precipitate was purified by recrystallization from CH_2Cl_2/Et_2O, to give $\mathbf{1}^{+}\bullet\mathbf{TCNQ}^{\bullet-}$ as blue crystals (137 mg, 87%). $\mathbf{1}^{+}\bullet\mathbf{TCNQ}^{\bullet-}$: $C_{52}H_{88}N_5$; MW 783.31; mp: 89–90 °C; MS (FAB^{+}-MS): *m/z* 578.66 ($[C_{40}H_{84}N]^{+}$); MS (FAB^{-}-MS): *m/z* 204.04 ($[C_{12}H_4N_4]^{-}$); IR (KBr): 2924 (s), 2855 (s), 2176 (s), 1585 (s), 1502 (s), 1362 (s), 1177 (s), 982 (m), 725 (m) cm^{-1}; Anal. Calcd. for $C_{52}H_{88}N_5$: C, 79.73; H, 11.32; N, 8.94. Found: C, 79.66; H; 11.27; N, 9.04.

Crystallographic Data of for $\mathbf{1}^{+}\bullet\mathbf{TCNQ}^{\bullet-}$: Deposition number 2312363 for $\mathbf{1}^{+}\bullet\mathbf{TCNQ}^{\bullet-}$ contain the supplementary crystallographic data for this paper. These data were provided free of charge by the joint Cambridge Crystallographic Data Centre and Fachinformationszentrum Karlsruhe Access Structures service.

Statement About Movie S1 (Supporting Information) and Figure 2b: The movie was taken using an ARTRAY ARTCAM-0016TNIR InGaAs camera (SWIR imaging camera) equipped with a LM25HC-SW lens under 1200 nm light (generated from halogen light source through a band-pass filter of 1200 nm). Liquid $\mathbf{1}^{+}\bullet\mathbf{TCNQ}^{\bullet-}$ at 70 °C, prepared by cooling the melted state generated above 90 °C, was adjusted to the shape of an arrow using a cover glass (coupled with rectangular and triangle glasses). The weak needlestick stimulation using a steel needle was applied on the cover glass at 70 °C. SWIR images of Figure 2b were clipped from Movie S1 (Supporting Information).

Statement About Movie S2 (Supporting Information) and Figure 6a: The movie was taken using an ARTRAY ARTCAM-0016TNIR InGaAs camera (SWIR imaging camera) equipped with a LM25HC-SW lens under 1200 nm light (generated from halogen light source through a band-pass filter of 1200 nm). The initial two drops of liquid of $\mathbf{1}^{+}\bullet\mathbf{TCNQ}^{\bullet-}$ at 70 °C on the glass substrate were prepared by heating the solid over 90 °C and subsequent cooling. The materials were covered with two round-shaped glasses. The weak and needlestick stimulations at 70 °C were applied to the sample on the left, whereas no needlestick stimulations were applied to the sample on the right. SWIR images of Figure 6a were clipped from Movie S2 (Supporting Information).

Supporting Information

Supporting Information is available from the Wiley Online Library or from the author.

Acknowledgements

This work was supported by JSPS KAKENHI (grant numbers, JP20H02692 and JP21H05486 to S.S., and JP20H02753 to T.N.), and Tokyo Ohka Foundation for The Promotion of Science and Technology (to S.S.). The authors thank Dr. Hiroyasu Sato (Rigaku) for the help of the X-ray crystal structure analysis for $\mathbf{1}^{+}\bullet\mathbf{TCNQ}^{\bullet-}$.

Conflict of Interest

The authors declare no conflict of interest.

Data Availability Statement

The data that support the findings of this study are available in the supplementary material of this article.

Keywords

π-dimerization, mechanochromism, phase transition, radical ion, shortwave infrared light transparency

Received: December 12, 2023
Revised: March 15, 2024
Published online:

[1] a) *Magnetism: Molecules to Materials II* (Eds.: J. S. Miller, M. Drillon), Wiley-VCH, Weinheim, Germany, **2001**; b) A. I. Taponen, A. Ayadi, M. K. Lahtinen, I. Oyarzabal, S. Bonhommeau, M. Rouzières, C. Mathonière, H. M. Tuononen, R. Clérac, A. Mailman, *J. Am. Chem. Soc.* **2021**, *143*, 15912.

[2] a) S. K. Pal, M. E. Itkis, F. S. Tham, R. W. Reed, R. T. Oakley, R. C. Haddon, *Science* **2005**, *309*, 281; b) T. Sugawara, H. Komatsu, K. Suzuki, *Chem. Soc. Rev.* **2011**, *40*, 3105; c) T. Suemune, K. Sonoda, S. Suzuki, H. Sato, T. Kusamoto, A. Ueda, *J. Am. Chem. Soc.* **2022**, *144*, 21980.

[3] a) Y. Morita, S. Nishida, T. Murata, M. Moriguchi, A. Ueda, M. Satoh, K. Arifuku, K. Sato, T. Takui, *Nat. Mater.* **2011**, *10*, 947; b) K. Hatakeyama-Sato, K. Oyaizu, *Chem. Rev.* **2023**, *123*, 11336.

[4] C. Shu, Z. Yang, A. Rajca, *Chem. Rev.* **2023**, *123*, 11954.
[5] a) T. Kusamoto, H. Nishihara, *Nature* **2018**, *563*, 480; b) R. Matsuoka, S. Kimura, T. Miura, T. Ikoma, T. Kusamoto, *J. Am. Chem. Soc.* **2023**, *145*, 13615.
[6] a) Y. Ikebata, Q. Wang, T. Yoshikawa, A. Ueda, T. Murata, K. Kariyazono, M. Moriguchi, Y. Morita, H. Nakai, *NPJ Quantum. Mater.* **2017**, *2*, 27; b) J. S. Park, J. Park, Y. J. Yang, T. T. Tran, I. S. Kim, J. L. Sessler, *J. Am. Chem. Soc.* **2018**, *140*, 7598.
[7] P. M. Beaujuge, S. Ellinger, J. R. Reynolds, *Nat. Mater.* **2008**, *7*, 795.
[8] a) S. Suzuki, D. Yamaguchi, Y. Uchida, T. Naota, *Angew. Chem., Int. Ed.* **2021**, *60*, 8284; b) S. Suzuki, D. Yamaguchi, Y. Uchida, T. Naota, *Angew. Chem.* **2021**, *133*, 8365; c) S. Suzuki, R. Shu, T. Naota, *Small* **2023**, *20*, 2305668.
[9] a) T. Kobashi, D. Sakamaki, S. Seki, *Angew. Chem., Int. Ed.* **2016**, *55*, 8634; b) T. Kobashi, D. Sakamaki, S. Seki, *Angew. Chem.* **2016**, *55*, 8634; c) K. Oda, S. Hiroto, H. Shinokubo, *J. Mater. Chem. C* **2017**, *5*, 5310; d) S. Suzuki, R. Maya, Y. Uchida, T. Naota, *ACS Omega* **2019**, *4*, 10031; e) T. Nishiuchi, S. Aibara, H. Sato, T. Kubo, *J. Am. Chem. Soc.* **2022**, *144*, 7479.
[10] a) S. Suzuki, T. Sakai, S. Takagi, T. Naota, *Angew. Chem., Int. Ed.* **2023**, *62*, e202308570; b) S. Suzuki, T. Sakai, S. Takagi, T. Naota, *Angew. Chem.* **2023**, *135*, e202308570.
[11] a) H. Ito, M. Muramoto, S. Kurenuma, S. Ishizaka, N. Kitamura, H. Sato, T. Seki, *Nat. Commun.* **2013**, *4*, 2009; b) T. Seki, K. Sakurada, H. Ito, *Angew. Chem., Int. Ed.* **2013**, *52*, 12828; c) T. Seki, K. Sakurada, H. Ito, *Angew. Chem.* **2013**, *125*, 13062; d) K. Chung, M. S. Kwon, B. M. Leung, A. G. Wong-Foy, M. S. Kim, J. Kim, S. Takayama, J. Gierschner, A. J. Matzger, J. Kim, *ACS Cent. Sci.* **2015**, *1*, 94; e) D. Zhang, S. Suzuki, T. Naota, *Angew. Chem., Int. Ed.* **2021**, *60*, 19701; f) D. Zhang, S. Suzuki, T. Naota, *Angew. Chem.* **2021**, *133*, 19853; g) M. Yoshida, V. Sääsk, D. Saito, N. Yoshimura, J. Takayama, S. Hiura, A. Murayama, K. Põhako-Esko, A. Kobayashi, M. Kato, *Adv. Opt. Mater.* **2022**, *10*, 2102614.
[12] a) J. Fabian, H. Nakazumi, M. Matsuoka, *Chem. Rev.* **1992**, *92*, 1197; b) G. Qian, Z. Y. Wang, *Chem. Asian J.* **2010**, *5*, 1006; c) Z. Sun, Q. Ye, C. Chi, J. Wu, *Chem. Soc. Rev.* **2012**, *41*, 7857.
[13] M. Yousaf, M. Lazzouni, *Dyes Pigm.* **1995**, *27*, 297;
[14] M. E. Itkis, X. CHI, A. W. Cordes, R. C. Haddon, *Science* **2002**, *296*, 1443.
[15] a) L. R. Melby, R. J. Harder, W. R. Hertler, W. Mahler, R. E. Benson, W. E. Mochel, *J. Am. Chem. Soc.* **1962**, *84*, 3374; b) Y. Iida, *Bull. Chem. Soc. Jpn.* **1969**, *42*, 71; c) J.-M. Lü, S. V. Rosokha, J. K. Kochi, *J. Am. Chem. Soc.* **2003**, *125*, 12161; d) A. L. Sutton, B. F. Abrahams, D. M. D'Alessandro, T. A. Hudson, R. Robson, P. M. Usov, *CrystEngComm* **2016**, *18*, 8906.
[16] S. Park, K. Fukuda, M. Wang, C. Lee, T. Yokota, H. Jin, H. Jinno, H. Kimura, P. Zalar, N. Matsuhisa, S. Umezu, G. C. Bazan, T. Someya, *Adv. Mater.* **2018**, *30*, 1802359.
[17] S. Tsuchiya, S. Susumu, *Jpn. Kokai Tokkyo Koho JP1985-286088*, Matsushita Electric Industrial Co., Ltd, Osaka, Japan, **1985**.
[18] K. Nishimura, G. Saito, *Synth. Met.* **2005**, *153*, 385.
[19] A. Bondi, *J. Phys. Chem.* **1964**, *68*, 441.